Journal of Virology

Virology | Full-Length Text

The role of HPV11 E7 in modulating STING-dependent interferon β response in recurrent respiratory papillomatosis

Lijuan Chen,[1,2] Huiying Hu,[1,2] Yufei Pan,[1,2] Yuanyuan Lu,[1,2] Mengyuan Zhao,[1,2] Yun Zhao,[2] Lixin Wang,[2] Kai Liu,[1,2] Zhenkun Yu[1,2]

AUTHOR AFFILIATIONS See affiliation list on p. 14.

ABSTRACT Recurrent respiratory papillomatosis (RRP) is a rare benign tumor caused mainly by the infection of the respiratory tract epithelial cells by the human papillomavirus (HPV) type 6/11. However, the specific mechanisms underlying the inhibition of the host's innate immune response by HPV remain unclear. For this purpose, we employed single-cell RNA sequencing to analyze the states of various immune cells in RRP samples post-HPV infection and utilized a cellular model of HPV infection to elucidate the mechanisms by which HPV evades the innate immune system in RRP. The results revealed distinct immune cell heterogeneity in RRP and demonstrated that HPV11 E7 can inhibit the phosphorylation of the stimulator of interferon genes protein, thereby circumventing the body's antiviral response. *In vitro* co-culture experiments demonstrated that stimulation of macrophages to produce interferon-beta induced the death of HPV-infected epithelial cells, also reducing HPV viral levels. In summary, our study preliminarily identifies the potential mechanisms by which HPV evades the host's antiviral immune response, as well as the latent antiviral functions exhibited by activated macrophages. This research serves as an initial exploration of antiviral immune evasion in RRP, laying a solid foundation for investigating immunotherapeutic approaches for the disease.

IMPORTANCE Surgical tumor reduction is the most common treatment for recurrent respiratory papillomatosis (RRP). One of the characteristics of RRP is its persistent recurrence, and multiple surgeries are usually required to control the symptoms. Recently, some adjuvant therapies have shown effectiveness, but none of them can completely clear human papillomavirus (HPV) infection, and thus, a localized antiviral immune response is significant for disease control; after all, HPV infection is limited to the epithelium. Inhibition of interferon-beta (IFN-β) secretion by HPV11 E7 viral proteins in epithelial cells by affecting stimulator of interferon genes phosphorylation may account for the persistence of low-risk HPV replication in the RRP. Moreover, suppression of the IFN-I pathway in RRP cell types might provide clues regarding the hyporeactive function of local immune cells. However, activation of macrophage groups to produce IFN-β can still destroy HPV-infected cells.

KEYWORDS HPV11E7, STING, RRP, scRNA - Seq, immunomodulation

Recurrent respiratory papillomatosis (RRP) is a rare, benign tumor mainly caused by persistent infection with low-risk human papillomavirus (HPV) types 6 or 11 (1). Patients with RRP exhibit a permissive innate response that supports chronic HPV infection and hampers virus clearance (2). For example, RRP presents an interleukin-10 (IL-10)-enriched microenvironment, which inhibits dendritic cell expression of proinflammatory cytokines to impair the development of anti-HPV immunity (3). Additionally, the Langerhans cells of papillomas display an immature state to express TH2-like and suppressor $CD4^+$ T cells in RRP (4). Given the ability of HPV to compromise innate

Editor Lawrence Banks, International Centre for Genetic Engineering and Biotechnology, Trieste, Italy

Address correspondence to Kai Liu, assimy1986@126.com, or Zhenkun Yu, yuzhenkun65@hotmail.com.

Lijuan Chen, Huiying Hu, and Yufei Pan contributed equally to this article. Author order was determined based on their contribution.

The authors declare no conflict of interest.

See the funding table on p. 15.

Received 13 December 2023
Accepted 26 March 2024
Published 16 April 2024

immune responses, there is a pressing need to better understand local cell-mediated antiviral defenses in RRP.

The type I interferon beta (IFN-β) plays a vital role in the forefront of host defense against pathogens and is a pivotal element in controlling viral infections, using multiple strategies to activate innate and adaptive immune cells (5). As a result, the virus must encode specific proteins to inhibit the activation of IFN-β and maintain its replication. Recently, viral proteins in HPV were reported to selectively target nucleic acid-sensing protein complexes, including the stimulator of interferon genes (STING) complex, which strengthens the ability of the virus to control host immunity (6). In addition to their antiviral capabilities, IFN-β exhibits anti-proliferative and apoptotic functions in viral infections, including the Encephalomyocarditis (EMC) virus, vesicular stomatitis virus (VSV), Herpes simplex virus (HSV), and hepatitis C virus (HCV) (7), and *in vitro* in cancer cell lines, including breast and prostate cancer cell lines. Treatment with crude IFN-I preparations has direct antiproliferative and cell cycle modulatory effects (8). Therefore, IFNs are widely used as therapeutics in clinics. Viruses infect host cells. Macrophages, as early producers of IFN-β, trigger other macrophages and nearby immune cells to secrete large amounts of proinflammatory cytokines to defend against viruses with different mechanisms (5). For example, macrophage-expressed IFN-β results in apoptosis of influenza virus-infected alveolar epithelial cells and produces proinflammatory cytokines to defend against severe acute respiratory syndrome coronavirus (9). The role of IFN-β and macrophages in RRP in intrinsic antiviral immunity remains unclear.

Human papillomavirus is a double-stranded DNA virus comprising more than 400 types, which causes infection of the genital or oral mucosa and is the causative agent of almost all cervical cancers, head and neck cancers, genital warts, and RRP (10). The oncogenic properties of high-risk HPV depend on two viral oncogenes, E6 and E7 (11), and the low-risk HPV6 and HPV11 genotypes will be investigated in this study. Repeated infections with low-risk HPV types 6 and 11 drive epithelial differentiation, which upregulates viral DNA replication and early E6 and E7 gene expression (12). Similar to other DNA viruses, these early genes can subvert immune responses by inhibiting interferon synthesis and signaling (8). Upon viral invasion, pattern recognition receptors identify pathogen-associated molecular patterns. This triggers the activation of the DNA sensor cyclic GMP-AMP synthase (cGAS), which produces the second messenger 2′,3′-cyclic GMP-AMP (cGAMP). Subsequently, cGAMP binds to the double-stranded DNA, activating STING and initiating downstream IFN-β activation (13). High-risk HPV type 16 E7 binds to interferon regulatory factor 9 (IRF-9) (14), impairing its nuclear translocation and attenuating IFN-I transcription. Human papillomavirus 18 E7 directly binds to the STING protein via its LXCXE motif to inhibit the downstream response (15). The effects of low-risk type HPV6/11 E7 remain poorly understood relative to those of HPV16 or HPV18 (12, 14)

Much of the current research focuses on the activation and dysfunction of immune cells in the RRP immune milieu and does not explain why local immunity remains depressed in the presence of large amounts of viral antigens. To address this knowledge gap, our study focused on cellular immune escape in HPV infection through manipulation of the STING/IFN-I pathway. Therefore, our study sought to annotate the landscape of IFN-β antiviral responses in the immune microenvironment of dysregulated RRPs and to reveal the mechanisms by which HPV6/11 evades STING-induced IFN-I activation.

MATERIALS AND METHODS

Human specimens

Twenty-seven clinical samples were obtained from patients with RRP after obtaining informed consent. Papilloma samples were collected from patients with RRP. Four papilloma and three normal mucosal samples were subjected to transcriptome profiling by single-cell RNA sequencing (scRNA-Seq). The clinical characteristics of all the samples used in this study are summarized in Table S1.

Single-cell RNA sequencing data processing and analysis

Fresh biopsies of the four RRPs were collected from the primary papilloma during surgical resection. Three pharyngopalatine arch mucosa samples were obtained from tonsil hypertrophy as a comparative group, and each tissue was separated into extra pieces and sent for pathological analysis. Seven samples were loaded onto the 10× genomics chromium single-cell platform, and libraries were sequenced using an Illumina platform with 150 bp pair-end sequencing. FASTQ with default parameter filtering of the adaptor sequence was applied, and low-quality reads were removed. Then, feature - barcode matrices were obtained by aligning reads to the human genome (GRCh38 Ensemble: version 100) using the package CellRanger. Next, downsampling analysis was performed among samples sequenced according to the mapped barcoded reads per cell of each sample, and finally, an aggregated matrix was obtained. The mitochondrial genes were removed from the expression tables. Further analyses were performed using the Seurat software package. For the quality control of the original data, the quality control conditions are the number of genes expressed by a single cell between 500 and 6,000, the unique molecular identifier (UMI) number >500, and the ratio of phosphorus gene expression <20%. Based on the expression table according to the UMI counts of each sample and the percentage mitochondrial rate, raw feature counts were log-normalized, scaled, and subjected to principal component analysis, which was performed based on the scaled data of the top 2,000 highly variable genes. The top 10 principal components (PCs) were used for TSNE and UMAP construction, and the unsupervised cell cluster results based on the top 10 PCs were obtained using a graph-based cluster method.

Differential gene expression analysis

To identify differentially expressed genes among the groups (RRP vs control; cells vs cells), the FindMarkers function with the Wilcoxon rank- sum test was used. Differentially expressed genes meeting the following criteria were selected: lnFC > 0.25, $P < 0.05$, and min. Pct >0.1. All processes were performed using the Novogene Cloud Analysis platform.

Tissue and primary cell suspension immunofluorescence staining

Formalin-fixed paraffin-embedded papilloma blocks were cut into 2 µm sections and placed on slides. Sections were deparaffinized and rehydrated, heat-induced epitope retrieval was performed, and the sections were permeabilized with PBS containing 0.01% Triton. Samples were stained with primary antibodies (HPV, Abcam) (IFN-β, Proteintech) for 12 h at 4°C. The sections were then stained with fluorescently labeled secondary antibodies (anti-rabbit, anti-mouse, Thermo Scientific) for 30 min at room temperature, washed three times with PBS, and stained with DAPI (Thermo Scientific) for 10 min. For immunofluorescence of suspension cells, the tissues were first dissociated into single-cell suspensions (Miltenyi Biotec) and seeded into 6-well plates for 12 h. On the second day, the experimental group was stimulated with 2′,3′-cGAMP (MCE) (Lipo3000 is required for stimulation to improve 2′,3′-cGAMP transfection efficiency) for 2 h, and the control group was stimulated with an incomplete medium for 2 h. Cells were fixed using 400 µL of 4% paraformaldehyde for 10 min at 37°C. The paraformaldehyde solution was removed, and the cells were washed three times with PBS. These steps were identical to those used for tissue immunofluorescence after heat-induced epitope retrieval. Images were captured using a confocal immunofluorescence microscope (OlyVIA; Olympus).

Enzyme-linked immunosorbent assay

Interferon-β levels in tissue and cell-culture media were measured using an IFN-β enzyme-linked immunosorbent assay kit (ABclonal) according to the manufacturer's instructions.

Viral load of HPV

The clone plasmids PUC57-HPV6E7-GFP and PUC57-HPV11E7-GFP (GenBank accession no.: AY492337.1 and KC329915) were produced by General Biol Co., Ltd., and the plasmid was extracted using a mini plasmid kit (Tiangen). After preparing the calibrators, we generated HPV6 E7 and HPV11 E7 calibration curves by qPCR using a range of HPV6 E7 and HPV11 E7 dilutions, as appropriate. The standard solution was diluted from $\times 10^{-1}$ to $\times 10^{-5}$. Differently diluted solutions were adjusted to the same volume and prepared in the same PCR master mix. The calibrator was subjected to PCR cycling under the conditions appropriate for amplifying the genes of interest, and each cycle was performed as per standards. A calibration curve was generated based on the cycles (16). To calculate the HPV load of clinical samples, we first determined HPV infection type 6 or 11 (cycle number < 30 indicates positive) and then determined the count of HPV6 E7 and HPV11 E7 (cycle number < 23 indicates positive). The primers used for each HPV type were as follows:

HPV6: forward 5′-TGCAACGACCATAGACCA-3′, reverse 5′-GCATATCCAGCATAATCAAAGT-3′;

HPV11: forward 5′-CGAGCAGACGTCCGTCCTCG-3′, reverse 5′-GGAATACATGCGCCATGTGG-3′;

HPV11 E7: forward 5′-CTGACCCTGTAGGGTTACATTG-3′, reverse 5′-CGCAGATGGGACACACAATA-3′; and

HPV6 E7: forward 5′-GTATTAGACCTGCAACCTCCAG-3′, reverse 5′-TGCACTTCTCTGATGTCTGTTT-3′.

The total DNA of each sample was extracted (Tiangen), and the total amount was set to be the same. Polymerase chain reaction was then performed to determine the number of cycles. The PCR conditions were the same as those used for plasmid PCR, and the primers were designed according to the sequence expressed by the plasmid. The number of cycles obtained was introduced into the algorithm using a standard curve to obtain the HPV6 E7 or HPV11 E7 load in the sample. Simple calculations were performed as previously described (17, 18).

Cell culture

The human head and neck squamous cell carcinoma cell line SNU-1076 was provided by Dr. Yanxiao from the ENT Center of Tongren Hospital affiliated with Capital Medical University, Beijing, China. The human monocyte cell line THP-1 was purchased from the Chinese Academy of Sciences, Shanghai, China. The cells were cultured in RPMI1640 (Servicebio) supplemented with 10% fetal bovine serum (Gibco) and 1% penicillin-streptomycin-glutamine (Gibco) at or below 90% confluency to optimize the growth conditions. For macrophage generation, 3×10^5 THP-1 cells were seeded in 0.4 µm-sized pore inserts treated with 200 nM phorbol 12-myristate 13-acetate (Bio shark) for 48 h and polarized into macrophages. Macrophages and SNU-1076 cells were co-cultured using a non-contact Transwell system (Corning). Inserts containing THP-1 macrophages were transferred to 6-well plates seeded with SNU-1076 cells in advance and co-cultured. After 12 h of co-culture, macrophages were treated with 2′,3′-cGAMP (MCE) for 2 h, and the control group was stimulated with incomplete medium. SNU-1076 cells and cell suspensions were harvested for further analyses.

Lentiviral transduction and stable cell generation

Packaging of lentivirus and retroviruses that expressed CMV-HPV6 E7-ZsGreen-T2A-PURO and CMV-HPV11 E7-ZsGreen-T2A-PURO was conducted by General Biol Co., Ltd. The lentivirus-packaged sequencing was the same as that for the plasmid. Stable HPV6 E7 and HPV11 E7 cells (SNU-1076) were generated by lentiviral transduction, followed by puromycin selection (19). The cells were transduced, and empty vector constructs were used as negative controls. The minimum concentration at which puromycin killed the wild-type cells was determined before testing for positive transfection of the virus. The

titer of the transfected virus depends on the cell density; an MOI of 50 was determined as optimal for the transfected virus. For successful transfection, after adding the virus and co-infection reagent, cells were incubated for 24–48 h, and puromycin was added twice or thrice for screening. In general, puromycin was added twice at 24 h, and after two times, the experiment was performed according to the cell density. The cell line can be used immediately after the screening. Successfully constructed cells fluoresced as a solid green color.

Antibodies and reagents for western blotting

The following antibodies were used for western blot analysis: rabbit monoclonal antibody against phosphor-(ser366) STING (Cell Signaling Technology), rabbit monoclonal antibody against STING (ABclonal), rabbit monoclonal antibody against phosphor-(s396) IRF3 (Cell Signaling Technology), rabbit polyclonal antibody against IRF3 (ABclonal), rabbit monoclonal antibody against TANK-binding kinase 1 (TBK1) (ABclonal), rabbit monoclonal antibody against phosphor-TBK1 (Abcam), and rabbit monoclonal antibody against GAPDH (ABclonal).

Transfected cells were stimulated with 2′,3′-cGAMP (MCE) or incomplete medium. Cells were harvested and lysed in RIPA buffer, protease inhibitor cocktail (MCE), phosphatase inhibitors (MCE), and PMSF (MCE). After centrifugation, the cleared lysates were analyzed using SDS-PAGE and western blotting.

Antibodies for flow cytometry

Papilloma tissues were lysed using a single-cell suspension (Miltenyi Biotec). The cells were then washed three times with PBS. Samples were washed with FACS buffer (0.2% BSA, 0.02% NaN_3, and PBS) and labeled for 30 min at 4°C using the anti-human antibodies: anti-human CD45 EF450 (eBioscience), CD68 monoclonal antibody FITC (eBioscience), 7AAD (Invitrogen), and Annexin V-propidium iodide (Servicebio). Data were acquired using a cytometer (BD Biosciences) and analyzed using the FlowJo software.

Gene expression qPCR

Total RNA was extracted using the Cell/Tissue Total RNA Isolation Kit (Vazyme). The RNA concentration was measured using a NanoDrop spectrophotometer (Thermo Fisher Scientific). RNA was reverse transcribed into cDNA using HiScript QRT SuperMix for qPCR. The primers were synthesized by Integrated DNA Technologies as follows:

IFIT: forward 5′-CTCTCTCTGCTTCCTTCTTCAC-3′, reverse 5′-GTGCCATAATCTCTGTCCTACC-3′;

OAS2: forward 5′-CGCTCTCTTCTCTGGAACTAAC-3′, reverse 5′-GATGTCTGCCTCATCCTCTTAC-3′;

MX1: forward 5′-GGATTGGAACCATAGCTCTACC-3′, reverse 5′-GACCTTGCCTCTCCACTTATC-3′;

IL-6: forward 5′-CTCTGGGAAATCGTGGAAAT-3′, reverse 5′-CCAGTTTGGTAGCATCCATC-3′;

IL-1β: forward 5′-CCACAGACCTTCCAGGAGAATG-3′, reverse 5′-GTGCAGTTCAGTGATCGTACAGG-3′; and

IL-8: forward 5′-GAGAGTGATTGAGAGTGGACCAC-3′, reverse 5′-CACAACCCTCTGCACCCAGTTT-3′.

Hematoxylin-eosin staining and the ThinPrep cytologic test

Surgically excised papilloma specimens were embedded in paraffin for hematoxylin-eosin staining. The results were analyzed by a professional pathologist. The surgically excised specimens were prepared as single-cell suspensions, and the experimental group

was subjected to 2′,3′-cGAMP stimulation, and cells stimulated in an incomplete culture medium were used as the control group. The cell suspension was collected for liquid-based cytological analysis (20). The cell sections from the experimental and control groups were examined under a microscope to determine the number of koilocytes.

Statistics

All functional experiments were performed with at least three independent biological replicates, and the number of replicates is indicated in the figure legends. Statistical analyses of functional experiments were performed using GraphPad Prism 9.0. All histograms are presented as mean ± SEM. The Student's *t*-test was used for comparisons in experiments with two sample groups. Analysis of variance (ANOVA) was performed for experiments with more than two sample groups. Pearson's correction was used for correction analysis.

RESULTS

Association between IFN-β level, HPV load, and clinical severity

All clinical samples were obtained by surgical resection with histological features including koilocytosis, hyperkeratosis, and multinucleated cells (21) (Fig. 1A). The selected patients were aged 27 ± 17.1 (6–66) years and represented a mixture of adult- and juvenile-onset RRP, harbored RRP driven by HPV types 6 or 11, and displayed variable disease severity as measured by the number of clinically indicated interventions in the 12 months before biopsy and a total number of lifetime surgeries (Table S1). IFN-β serves as the major contributor in defending against viruses by obstructing the replication of numerous viruses (7). To better investigate whether this difference affects the local antiviral response, we examined the local tissue IFN-β levels as well as viral load in surgically resected tumors (Fig. 1B). Correlation analysis revealed that IFN-β levels in localized neoplasms were negatively correlated with viral load (for patients infected with both types 6 and 11, we combined the viral loads for the statistics) (Fig. 1C). The relationships among viral load, interferon levels, and clinical severity were evaluated. The clinical severity was evaluated based on the number of surgeries performed per year (Fig. 1B). Furthermore, correlation analysis found higher tissue IFN-β expression levels and lower viral loads in patients who experienced fewer clinical treatments in 1 year (Fig. 1D and E). Increased HPV load is highly likely to be an aggressive disease characteristic. Interferon-beta in the RRP microenvironment exerts disruptive effects on viral replication.

Single-cell RNA sequencing defines RRP cellular alterations and the antiviral functional landscape

STING is ubiquitously expressed by epithelial and immune cells, accompanied by the fact that both cancer and immune cells should produce IFN-β. To better identify the RRP microenvironment after HPV infection, we performed scRNA-Seq analysis and compared four HPV-infected RRP tissue samples with three pharyngopalatine arch mucosa samples from patients with tonsil hypertrophy who were not infected with HPV using the 10× genomics chromium platform (Fig. 2A). The clinical information is summarized in Table S1. After removing low-quality cells and potential doublets, 72,867 cells remained. We identified 12 clusters and annotated them using differentially expressed marker genes (Fig. S1A through C), including those of immune cells (B cells, T cells, mast cells, NK cells, NKT cells, and macrophages) and non-immune cells (basal cells, epithelial cells, endothelial cells, fibroblasts, keratinocytes, and mesenchymal cells). We then separated them into control and RRP groups (Fig. 2B). Compared to the control, the RRP group showed marked proportional alterations in the cell clusters (Fig. 2B and C). Among the 12 clusters, three, namely basal cells, epithelial cells, and koilocytes, derived from the basal layer of the epithelium, showed the greatest increase in RRP. All immune cell populations showed

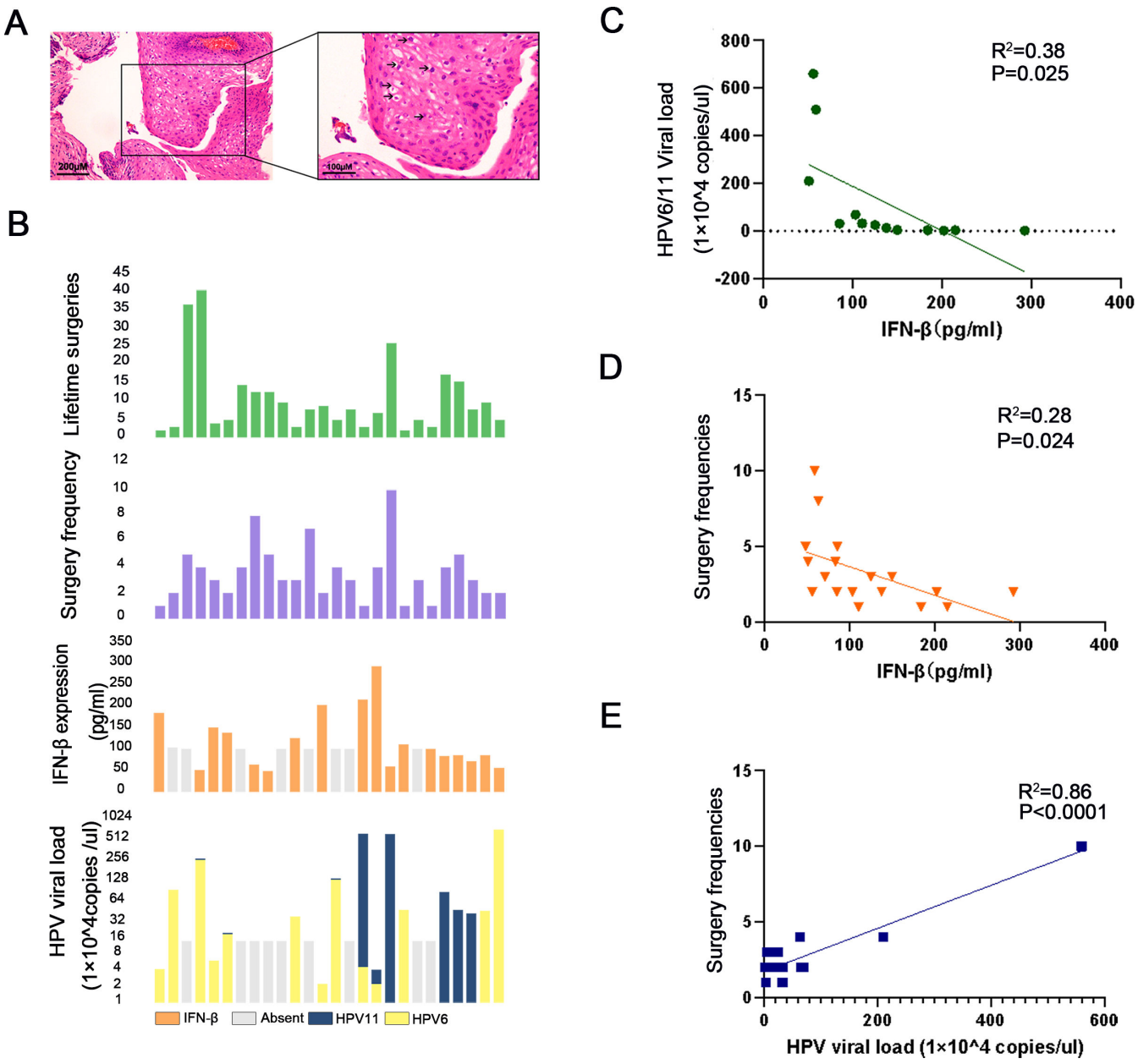

FIG 1 (A) Hematoxylin and eosin Stain (original magnification 200×) showing the cellular neoplasm with viral cytopathic effects, including irregular, raisinoid nuclei and koilocytes. (B) The bar plots represent the corresponding interferon-beta expression, HPV type, viral load, the total number of lifetime surgeries, and the number of surgeries in a year prior to biopsy for each patient. (C) Correlation analysis of the corresponding tissue interferon-beta expression with local HPV viral load (n = 13, Pearson correlation coefficient). (D) Correlation analysis of tissue IFN-β expression and surgeries' intervention in a year (n = 18, Pearson correlation coefficient). (E) Correlation analysis of tissue HPV viral load (patients co-infected with HPV11 and HPV6 were selected for comparison with the total viral load) and surgeries' intervention in a year (n = 17, Pearson correlation coefficient).

the opposite trend, except for macrophages, the proportion of which was the only upregulated immune cell population compared to that of the control (Fig. 2B and C). These findings present an alternative perspective on continuous HPV6 or HPV11 infections at local sites. Despite RRP presenting with HPV accumulation, the cells still showed a persistent absence of immune activity, with immune cell levels lower than typical post-infection levels (Fig. 2C). To explain this, we investigated the profile of the IFN-β activator, the STING pathway. Despite accumulating evidence demonstrating that high-risk HPV infection downregulates IFN-I expression in cervical or head and neck cancers, alterations in the immune response to RRP caused by HPV6 or HPV11 remain

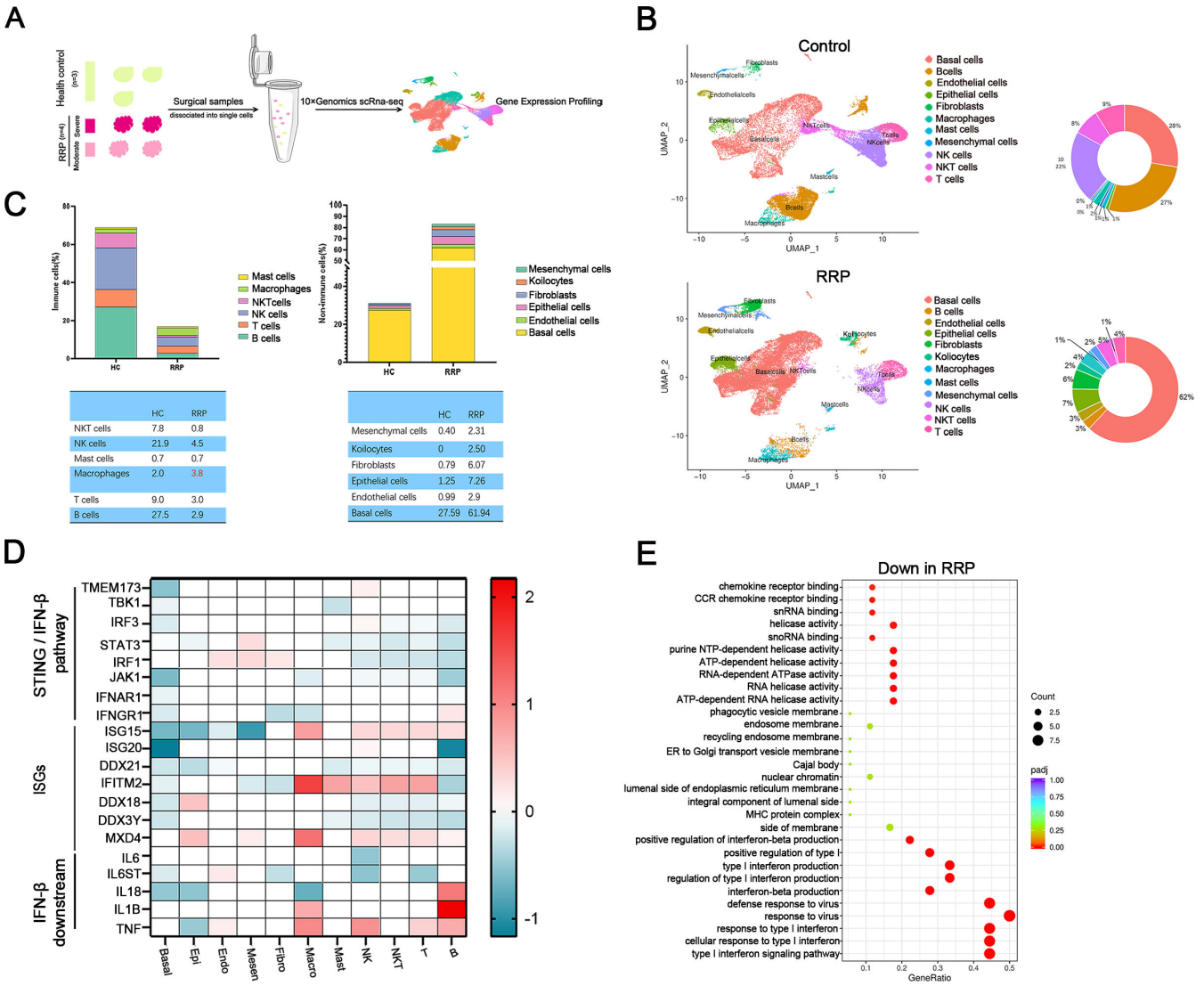

	HC	RRP
NKT cells	7.8	0.8
NK cells	21.9	4.5
Mast cells	0.7	0.7
Macrophages	2.0	3.8
T cells	9.0	3.0
B cells	27.5	2.9

	HC	RRP
Mesenchymal cells	0.40	2.31
Koilocytes	0	2.50
Fibroblasts	0.79	6.07
Epithelial cells	1.25	7.26
Endothelial cells	0.99	2.9
Basal cells	27.59	61.94

FIG 2 (A) Experimental scheme depicts the tissue harvesting for scRNA-Seq. RRP cells and pharyngopalatine arch mucosa cells were harvested, purified, and subjected to scRNA-Seq (n = 7). (B) UMAP plot displays the 11 major color-coded cell clusters in the control group (pharyngopalatine arch mucosa cells) and 12 major clusters in the RRP group. Pie charts display the proportion of each cell type in overall control group cells and RRP group cells by scRNA-Seq. (C) The column charts and tables show the ratio of immune cells and non-immune cells in the control groups and RRP groups. (D) Heatmap shows the average expression levels (color-scaled, row-wise Z scores) of the STING/IFN-β related genes (columns) across the cell clusters (rows). (E) KEGG analysis shows the downregulated signaling pathways.

poorly understood. We primarily mapped the STING pathway genes by patient identity, and RRP exhibited a large number of downregulated genes related to innate antiviral response (Fig. S1D). Kyoto Encyclopedia of Genes and Genomes (KEGG) analysis of the downregulated genes revealed that most pathways involved IFN-I response and antigen processing (Fig. S1E). We specifically analyzed IFN-I pathway-related genes, particularly the STING pathway, in each cell type. Consistent with the patient identity data, most STING pathway-related genes, Interferon-stimulated genes (ISGs), and downstream IFN-I cytokines were downregulated or not activated in almost all RRP cell types compared with the control (22). In particular, the epithelial and basal clusters barely demonstrated anti-viral gene activation (Fig. 2D and E). These data suggest that in RRP, not only is the infiltration of immune cells low in number but the STING/IFN-β pathway is also suppressed, possibly related to the low reactivity of RRP.

HPV11 E7 downregulates IFN-β responses by inhibiting STING phosphorylation

To further investigate the effect of HPV6 or HPV11 oncoproteins on antiviral functions in epithelial cells, we established a stable cell model expressing HPV6 or HPV11 E7 oncoproteins using the SNU-1076 cell line (19) (Fig. 3A; Fig. S2A). Human papillomavirus often employs strategies to counteract the host IFN-I response, thereby enhancing viral replication and integration. To identify whether HPV11 E7 and HPV6 E7 inhibit the downstream STING/IFN-β pathway, we initially treated HPV⁻ SNU-1076 cells with 2′,3′-cGAMP, an endogenous agonist of IFN-β (5) for 2 and 6 h. STING activation was observed at 2 h, which then decreased at 6 h (Fig. 3B). Quantitative enzyme-linked immunosorbent assay analysis of IFN-β protein levels showed a similar pattern, reaching

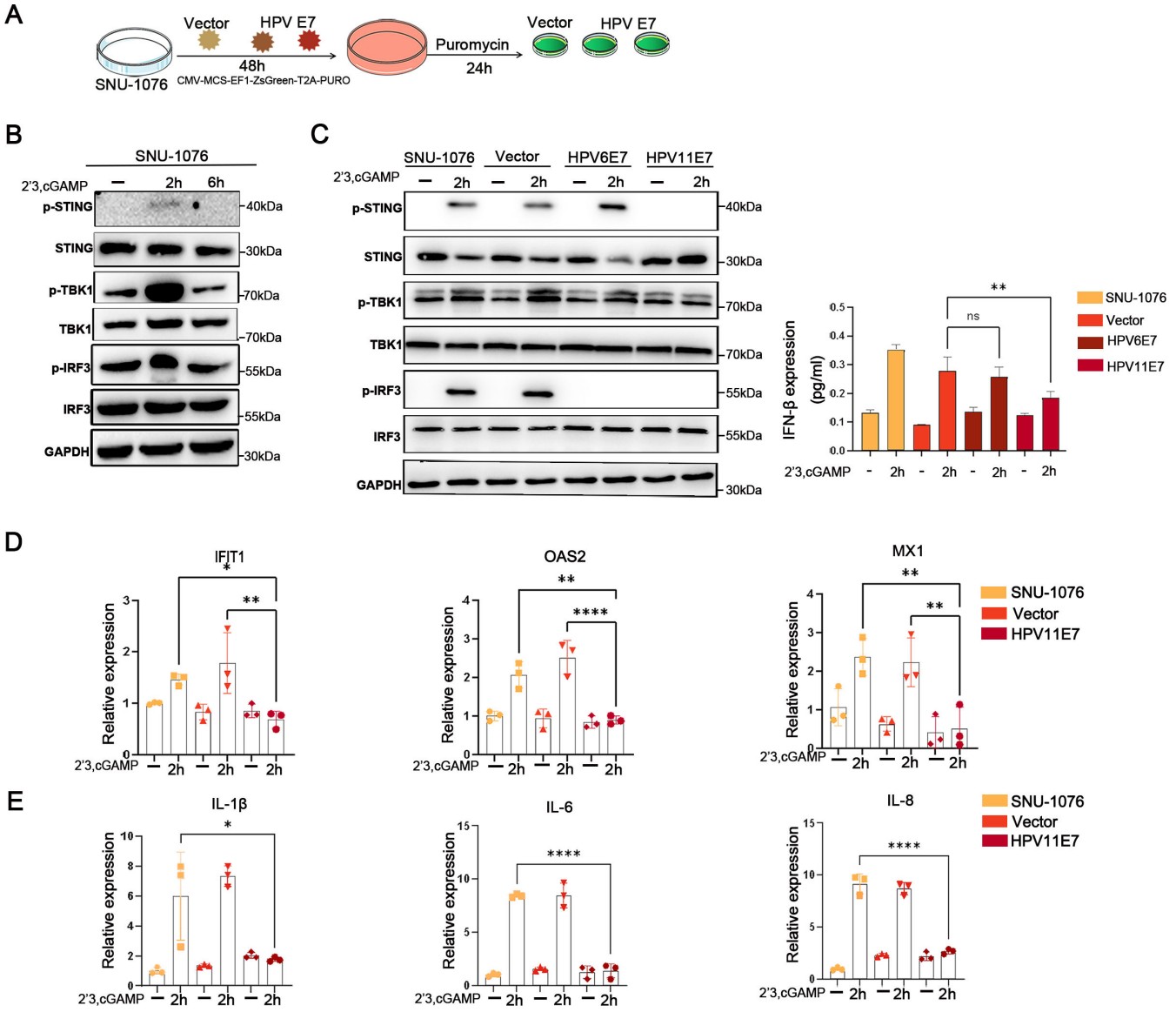

FIG 3 (A) Experimental scheme depicts the RRP model building process *in vitro*. (B) Immunoblot of SNU-1076 cell line used in panels C–E. (C) Western blot analysis of HPV11E7 and HPV6E7 stably infected SNU-1076 cell line treated with 2′,3′ cGAMP using indicated antibodies ($n = 3$); ELISA analysis of IFN-β level of cell supernatant in corresponding groups ($n = 3$,$^{**}P < 0.01$ and $^{*}P < 0.05$); statistic method is ordinary one-way ANOVA. (D) qPCR analysis of HPV11E7 stably infected SNU-1076 cell line with 2′,3′ cGAMP. Expression level of IFIT1 ($n = 3$, $^{**}P < 0.01$ and $^{*}P < 0.05$), OAS2 ($n = 3$, $^{**}P < 0.01$ and $^{****}P < 0.0001$), and MX1 ($n = 3$, $^{**}P < 0.01$). (E) qPCR analysis of HPV11E7 stably infected SNU-1076 cell line with 2′,3′ cGAMP. Expression level of IL-1β ($n = 3$, $^{*}P < 0.05$), IL-6 ($n = 3$, $^{****}P < 0.0001$), and IL-8 ($n = 3$, $^{****}P < 0.0001$). Data are represented as mean ± SEM; statistic method is ordinary one-way ANOVA.

the highest levels at 2 h (Fig. S2B). These results suggest that activation of the STING pathway to induce IFN-β is normal in the absence of HPV. We examined the STING pathway in HPV11 E7-transfected SNU-1076 cells stimulated with 2′,3′-cGAMP for 2 h. To exclude the influence of viral capsids, we included an empty vector control group. STING, TBK1, and IRF3 protein levels did not show significant changes in HPV11 E7-transfected cells, which was consistent with our results of scRNA-Seq analysis for transcriptional expression (Fig. 2D and 3C). The cellular experiments exhibit the transcriptional levels associated with the STING pathway, which vary from RRP patient samples. Genes IRF1, JAK1, STAT3, and IRF2 are known STING signaling targets that showed substantial variability between RRP samples. The second patient's sample demonstrated markedly lower expression of anti-viral related genes in comparison to other RRP patient samples (Fig. S1D). However, the phosphorylation of STING, TBK1, and IRF3 noticeably decreased (Fig. 3C). This indicates that inhibition of the STING pathway is primarily due to the suppression of STING phosphorylation. Similarly, the levels of secreted IFN-β showed significant suppression in HPV11 E7-expressing cells (Fig. 3C). Activation of the STING pathway represents a relatively initial step for the induction of IFN-β. When we analyzed the mRNA expression of downstream ISGs and cytokines, including IFIT1, MX1, OAS2, IL-1β, IL-6, and IL-8, which are essential IFN-I target genes (22), we observed a significant decrease in ISGs. The transcription levels of these cytokines were repressed in HPV11 E7-expressing cells after treatment with 2′,3′-cGAMP (Fig. 3D and E). These data indicated that HPV11 E7 potently suppressed STING-induced immune activation. Regarding the effect of HPV6 E7 on the interferon response, in epithelial cells transfected with HPV6 E7 after stimulation with 2′,3′-cGAMP for 2 h, we observed that the phosphorylation of IRF3 (p-IRF3) was inhibited, whereas the activation of other proteins remained unaffected (Fig. 3C). The levels of IFN-β in the supernatant of HPV6 E7-transfected cells did not show a significant decrease (Fig. 3C). Total protein levels were consistent with the single-cell transcriptional levels, with no noticeable changes observed (Fig. S2C).

Effects of macrophage-induced IFN-β on HPV-infected epithelial cells

Keratinocytes act as a first line of defense by separating the external environment from the internal environment, and they are born with pattern recognition receptors that allow them to recognize pathogens and initiate antiviral immunity (12). However, in HPV6- or HPV11-infected RRP, scRNA-Seq results indicated that the IFN-I response was inhibited in most cell types. We mapped the reads of all cell types to IFN-β expression and identified the location as macrophages in RRP and healthy tissue as a control (Fig. 4A; Fig. S4B). Coincidentally, macrophages represent the exclusively increased immune cell type in RRP, which simultaneously do not perform transcriptional repression of antiviral genes, similar to epithelial cells, and the activation markers are expressed normally (Fig. 2D; Fig. S3A). These results suggest that macrophages were activated (23). However, the antiviral STING pathway was not activated. Therefore, activating the STING pathway in macrophages might yield an unexpected effect on enhancing their antiviral capacity. In addition to the antiviral effect, IFN-β could also exert antiproliferative and proapoptotic functions to interrupt the virus replication strategy in host cells by inducing cell death (7). To further investigate the potential role of macrophage-induced IFN-β in RRP, we used the phorbol 12-myristate 13-acetate-differentiated THP-1 cell line as a macrophage model (24), co-cultured with HPV cells *in vitro* (Fig. 4B). Following THP-1 stimulation with 2′,3′-cGAMP, an endogenous agonist of IFN-β in mammalian cells, for 2 h, the IFN-β level in the cell supernatant was increased (Fig. 4B and C). We used the THP-1 co-culture system to culture the HPV11 E7/HPV6 E7 stably transfected SNU-1076 cell line with an incomplete culture medium as a control, and THP-1 co-cultured with vector and SNU-1076 as non-E7 control (Fig. 4B; Fig. S3C and D). The effects of macrophage-induced IFN-β on HPV-infected epithelial cells were evaluated by annexin V-propidium iodide staining and flow cytometry. Significantly higher cell death was observed in the 2′,3′-cGAMP cultured HPV11 E7/HPV6 E7 cells than in the control (Fig. 4D and E; Fig. S3B and E). To verify this effect in the RRP microenvironment, we

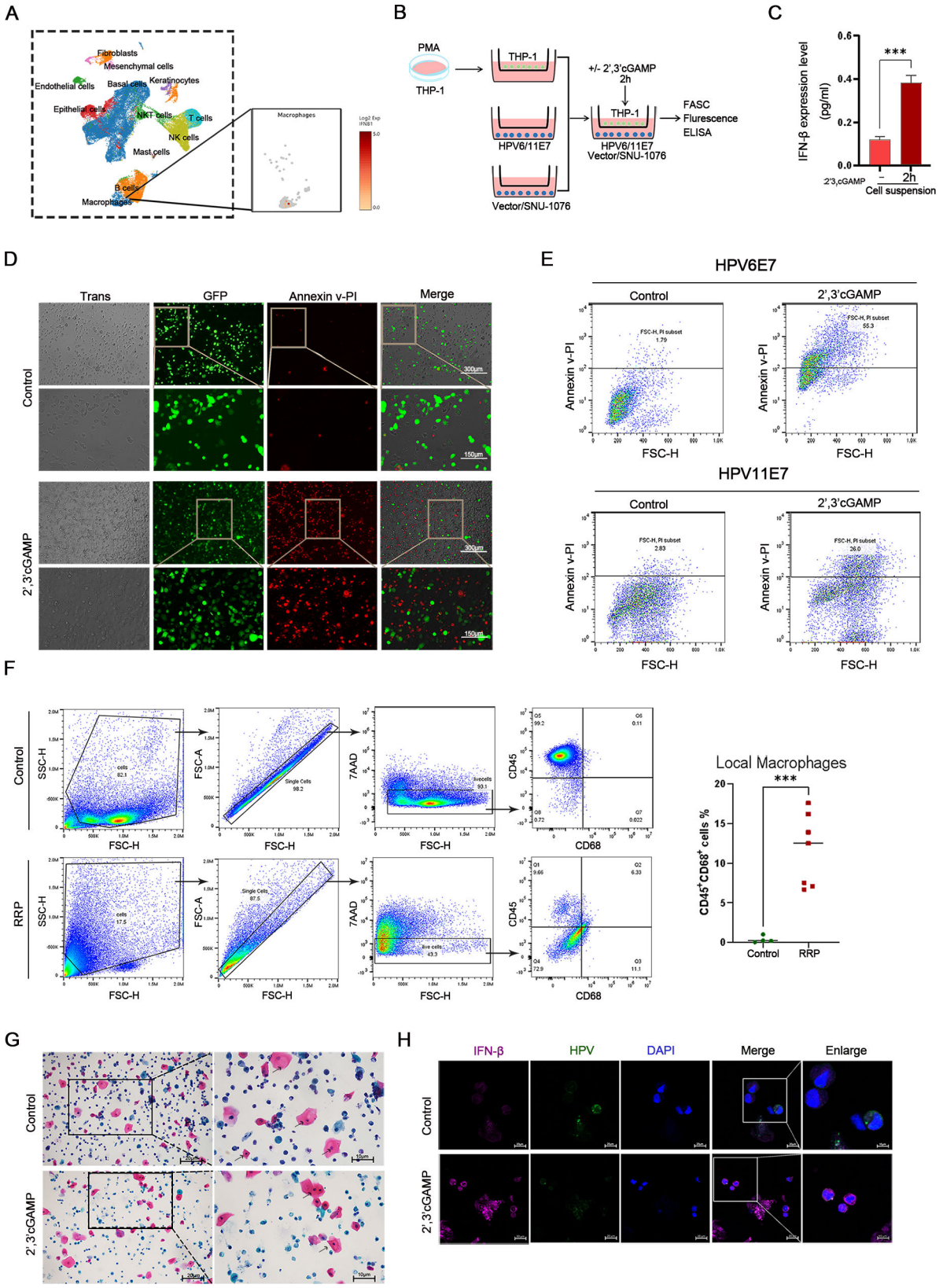

FIG 4 (A) UMAP plot displays IFN-β expression majorly located in macrophage cluster in RRP samples. (B) Depicting the procedure of co-culture of phorbol 12-myristate-13-acetate (PMA)-differentiated THP1 cells and HPV11E7-transfected SNU-1076 cell line. HPV11E7 cell viability was quantified by immune staining Annexin V-PI and flow cytometry. (C) ELISA analysis of with or without 2′,3′ cGAMP stimulated co-cultured cell supernatant IFN-β level. (D) Immune staining

(Continued on next page)

FIG 4 (Continued)

showed Annexin V-PI expression in HPV11E7 with or without 2′,3′ cGAMP stimuli. (E) Flow cytometry showed Annexin V-PI expression in HPV11E7 with or without 2′,3′ cGAMP stimuli (n = 3, $^{**}P < 0.01$). (F) Flow cytometry gating strategy of macrophage in primary RRP single cell suspension (n = 5) and healthy control sample (n = 3, $^{***}P < 0.001$, paired t-tests). (G) ThinPrep cytologic test represents the number of koilocytes in primary RRP cell suspension decreased after stimulation with 2′,3′ cGAMP. Control RRP cell suspension was stimulated with incomplete media. (H) Confocal fluorescent microscopy displays the intensity of IFN-β and HPV L1 after stimulation with or without 2′,3′ cGAMP.

first detected an increased number of macrophages in the RRP (Fig. 4F), consistent with scRNA-Seq results (Fig. 2D). Next, we treated 2′,3′-cGAMP to the single-cell suspension prepared using primary RRP tissue. The ThinPrep cytologic test, a detection method for atypical squamous cells in cervical cancer screening, which allows abnormal epithelial cells to be observed (20), was used to observe the changes in epithelial cells of RRP clearly after treatment. We found the 2′,3′-cGAMP treatment suspension had a reduced number of heterogeneous epithelial cells compared with the not-treated suspension (Fig. 4G; Fig. S3C). Furthermore, based on the negative correlation of HPV load and IFN-β expression (Fig. 1D), observation of the fixed RRP single cell suspension showed that the 2′,3′-cGAMP-stimulated suspension exhibited a decline in HPV protein expression with an increased IFN-β expression level (Fig. 4H; Fig. S3D). These data indicated that macrophage-produced IFN-β produced by STING activation contributes largely to the death of infected epithelial cells and destroys the HPV *in vitro*.

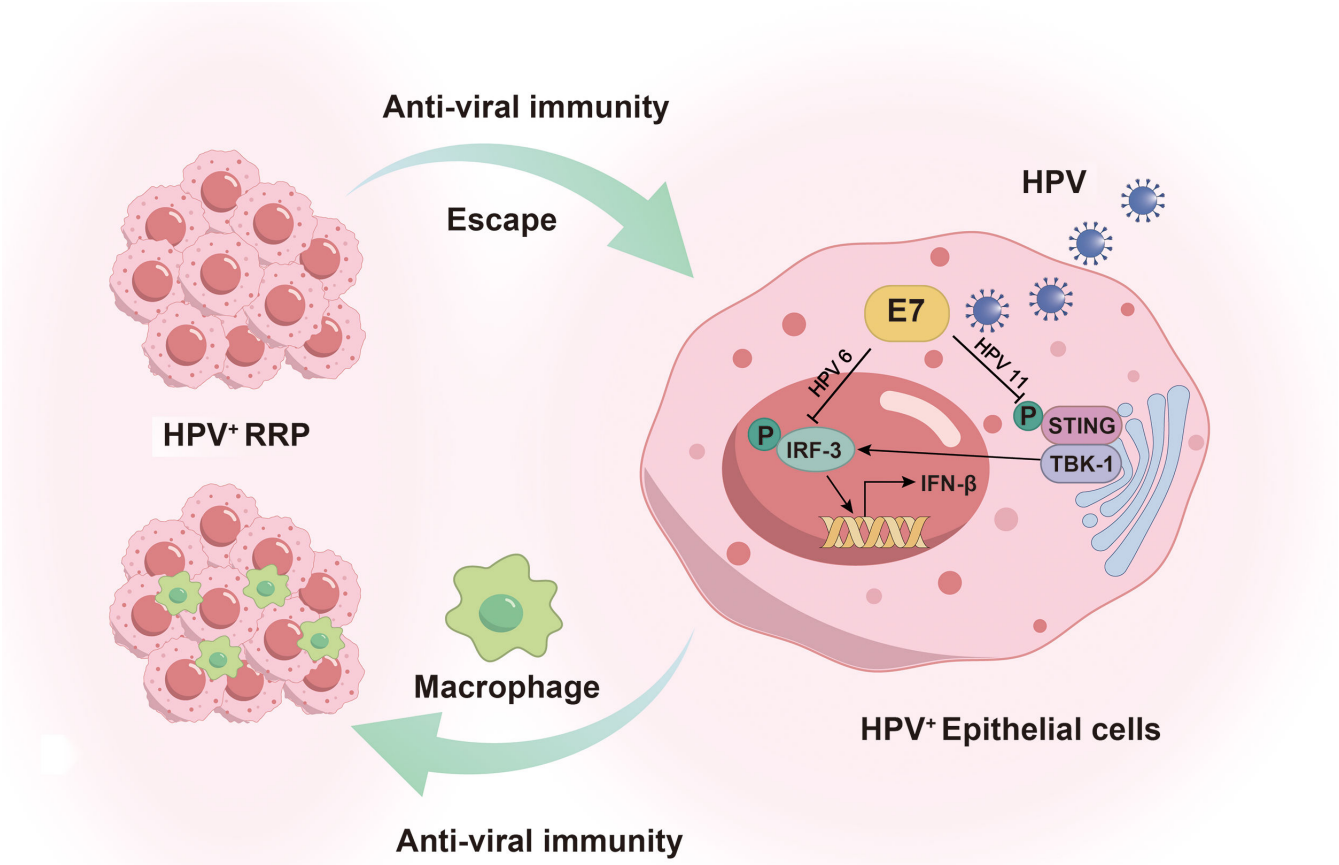

FIG 5 Schematic model of local immune regulation in RRP. Inhibiting STING phosphorylation by HPV11 E7 circumvents the body's antiviral response in epithelial cells. Stimulating macrophages to produce IFN-β induces the death of HPV-infected epithelial cells and reduces HPV viral levels.

DISCUSSION

In the RRP management landscape, which has historically emphasized surgical lesion excision, emerging therapies involving HPV vaccines and bevacizumab offer notable promise (25, 26). However, these therapies have not provided evidence of HPV particle clearance. Interferon-β serves as an antiviral agent with antiproliferation effects and the ability to activate adaptive immunity (7). Our study highlights the role of tissue IFN-β levels in RRP, clinical severity, and their correlation with HPV6/11 loads, thus emphasizing the importance of alternative treatment avenues. This sheds light on the antiviral immune mechanism of IFN-β in RRP.

To our knowledge, this is the first study employing scRNA-Seq to gain insights into RRP. The data revealed an apparent downregulation in the number of immune cell groups, except for macrophages. This aligns with previous research showing innate immunity defects in RRP, including Langerhans cells displaying diminished CD83 maturation markers and impaired killer cell immunoglobulin-like receptor gene haplotypes (4, 27, 28). Our data predominantly indicate a broader immune cell type alteration in RRP, consistent with the HPV-induced immunosuppressive environment, but also, at another level, explain the immunological condition of patients with RRP by altering the number of immune cells. Utilizing scRNA-Seq, we identified differential IFN-β-related gene expression across cell clusters. There is substantial variability in gene expression in the STING pathway in patient samples compared to the cell culture results. Specifically, we observed a downregulation of the IFN-β pathway starting from the upstream gene STING in epithelial cells, consistent with the downregulation of basal cells. This observation supports the involvement of the HPV oncoprotein in basal cells, which leads to the shutdown of host immune detection in basal cells that have the highest proportion of RRP. These results suggest that even if basal cells differentiate into epithelial cells, the virus is still affecting their function. Consistent with previous studies, post-HPV infection, the virus's life cycle uniquely adapts according to the maturity and differentiation of epithelial cells, thereby extending its own lifespan.

Like most DNA viruses, HPV subverts host immune surveillance by manipulating IFN signaling (29). Viral infection activates the cytosolic DNA to produce cGAS, which then induces cGAMP and finally activates STING. The activated STING protein recruits downstream TBK1 to the C-terminal tail (CTT) to form oligomers that allow the CTT-bound TBK1 to phosphorylate CTT that is not bound to TBK1 (30). The phosphorylated residues on the CTT represent a motif for the phosphorylation and translocation of IRF3 into the nucleus to induce IFN-β (31). Previous studies have shown that the cGAS/STING response does not occur at the initial stage of HPV infection (32), and based on our data, according to our experimental data, STING activation is inhibited in HPV-infected epithelial cells. Our study complements the role of HPV on STING in persistent HPV infection status. Human papillomavirus usually compromises the critical factor in this pathway (29). Our results show that STING can be activated in HPV6E7-transfected cells, while downstream phosphorylated IRF3 is not activated. This indicates that HPV6E7 uniquely influences the activation of phosphorylated IRF3, diverging for distinct reasons. One study found that high-risk HPV18E7 inhibited STING activation, and another found that STING activation was significantly elevated by the addition of 2′,3′ cGAMP to HPV31- and HPV16-transfected cells (6, 33). Such discrepancies underscore the heterogeneity in how different HPV strains modulate the STING pathway. Our findings also show such a manifestation. High-risk HPV16 or HPV18 is linked to the development of cervical cancer and head and neck squamous cell carcinoma (12). Oncoprotein E7 of high-risk HPV16 binds to IRF9, pRb, and IRF1 to prevent downstream cytokine transcription (34). In HPV16-positive head and neck squamous cell carcinomas, cGAS-STING responses are destroyed and restored when HPV16 E7 is lost (34). HPV18 E7 preferentially interacts with STING, the center of the DNA-sensing pathway (15). Oncoprotein E7 of low-risk HPV6 or HPV11 is less well known. Our study revealed that E7 of HPV11 prevents the IFN-β response by inhibiting the phosphorylation of STING *in vitro* in RRP, suggesting that even low-risk HPV11 E7 has the ability to interrupt the antiviral response in epithelial cells.

Our study also showed that STING and TBK1 activation was normal in another HPV6 E7 subtype, whereas IRF3 phosphorylation was abnormal. This suggests that HPV11 E7 might exert a stronger inhibitory effect on antiviral functions compared to HPV6 E7. This observation might also elucidate why patients infected with HPV11 tend to exhibit more severe clinical manifestations (35). Our data suggest that HPV6 and HPV11 may differentially affect the STING pathway. Both HPV6 and HPV11 viruses are non-carcinogenic group Alphapapillomaviruses (36). Some studies have identified infection with HPV11 as being associated with more aggressive disease and higher recurrence of lesions. And HPV6 gene sequences are four times more diverse than HPV11 types (37). They have more diversity in their gene sequences. Our data suggest that types 6 and 11 do not act the same way on STING, or it could be due to sequence differences, but the exact mechanism still needs to be further investigated.

In HPV-infected lesions, viral replication and protein production occur within the upper layers of the squamous epithelium, thereby upregulating the viral gene expression following keratinocyte differentiation (12). This process unfolds locally and is devoid of proinflammatory cytokines or infiltrated immune cells because local epithelial cells lose their interferon-secreting capacity (38). Consequently, cell-mediated immune response is crucial for viral clearance. Macrophages play a pivotal role in antiviral defense by promoting the removal of infected cells, antigen presentation, and expression of effector molecules for viral clearance. Notably, alveolar macrophage-derived IFN-β can induce alveolar epithelial cell injury via autocrine TNF-related apoptosis-inducing ligand induction (39). Combining probiotics with alveolar macrophage-derived IFN-β demonstrates the suppression of respiratory syncytial virus infection (40). Our findings suggest that the number of macrophages in the RRP group was elevated with uninhibited STING expression. Macrophage-secreted IFN-β contributes significantly to immune development and antiviral response.

IFN-β serves as a critical mediator of apoptosis in certain virus infections, such as EMC virus, VSV, and HSV, as evidenced by the inhibition of infected cell apoptosis when anti-IFN-α/β antibodies are introduced or when the IFN receptor or Stat-1 signaling factor is lacking in null cells (41). Interferons, particularly IFN-α, have been successfully used in clinical applications for hepatitis C and hepatitis B, Kaposi's sarcoma, genital warts, hairy cell leukemia, chronic myelogenous leukemia, and malignant melanoma (42). Early studies on RRP suggested that exogenous therapeutic IFN-α is not a curative or substantially beneficial adjunctive agent for long-term RRP management (25). Our study shows that stimulating macrophages to produce IFN-β induces the death of infected epithelial cells *in vitro*. Therefore, our data highlight the potential of macrophage-induced IFN-β in RRP as a novel strategy for treating HPV and papilloma infections.

In conclusion, our study utilized scRNA-Seq to elucidate the inhibitory antiviral function of HPV11 and HPV6 in RRP. We observed that HPV11 suppresses IFN-I in epithelial cells via the STING signaling pathway and identified a novel role for macrophage-induced IFN-β in potentially counteracting this mechanism, thereby laying the foundation for developing effective therapeutic interventions for HPV6- or HPV11-infected RRP(Fig. 5).

ACKNOWLEDGMENTS

This work was funded by Programs of the Jiangsu Provincial Commission of Health and Family Planning Funding (K2019015), the Foundation of Nanjing Medical University (NMUB20220141), the National Natural Science Foundation of Jiangsu (BK20231124), and Priority Academic Program Development of Jiangsu Higher Education Institutions.

AUTHOR AFFILIATIONS

[1]Department of Otolaryngology-Head and Neck Surgery, BenQ Medical Center, The Affiliated BenQ Hospital of Nanjing Medical University, Nanjing, Jiangsu, China

[2]Nanjing Medical Key Laboratory of Laryngopharynx-Head and Neck Oncology, Nanjing, Jiangsu, China

AUTHOR ORCIDs

Lijuan Chen http://orcid.org/0000-0002-0890-9994
Kai Liu http://orcid.org/0000-0002-6947-6758
Zhenkun Yu http://orcid.org/0009-0004-7648-0538

FUNDING

Funder	Grant(s)	Author(s)
The Jiangsu Provincial Commission of Health and Family Planning Funding	K2019015	Huiying Hu
The National Natural Science Foundation of Jiangsu	BK20231124	Zhenkun Yu
The Foundation of Nanjing Medical University and Academic program Development of Jiangsu Higher Education Institutions	NMUB20220141	Zhenkun Yu

DATA AVAILABILITY

The data supporting the findings of this study are available upon reasonable request. Single-cell RNA sequencing data from our research are loaded on Gene Expression Omnibus (GEO, accession numbers: GSE261589).

ETHICS APPROVAL

All patients provided informed consent preoperatively to participate in the study following relevant local, national, and international regulations at the Affiliated BenQ Hospital of Nanjing Medical University (Decision No. 2020-KL013).

ADDITIONAL FILES

The following material is available online.

Supplemental Material

Fig. S1 (JVI01925-23-s0001.tif). UMAP visualization, violin pot, heatmap analysis, and KEGG analysis.
Fig. S2 (JVI01925-23-s0002.tif). Fluorescence microscopy, ELISA, and densitometric analysis.
Fig. S3 (JVI01925-23-s0003.tif). Violin plot, UMAP plot, immune staining, and flow cytometry.
Supplemental legends (JVI01925-23-s0004.docx). Legends for Fig. S1 to S3.
Table S1 (JVI01925-23-s0005.docx). All patients' demographic and clinical data.

REFERENCES

1. Derkay CS, Bluher AE. 2019. Update on recurrent respiratory papillomatosis. Otolaryngol Clin North Am 52:669–679. https://doi.org/10.1016/j.otc.2019.03.011
2. Bonagura VR, Hatam LJ, Rosenthal DW, de Voti JA, Lam F, Steinberg BM, Abramson AL. 2010. Recurrent respiratory papillomatosis: a complex defect in immune responsiveness to human papillomavirus-6 and -11. APMIS 118:455–470. https://doi.org/10.1111/j.1600-0463.2010.02617.x
3. Rosenthal DW, DeVoti JA, Schmidtmayerova H, Steinberg BM, Bonagura VR. 2008. Human papillomavirus causes a T_H2 - Like chemokine predominance in recurrent respiratory papillomatotosis (RPR). J Allergy Clin Immunol 121:S15. https://doi.org/10.1016/j.jaci.2007.12.062
4. Israr M, DeVoti JA, Lam F, Abramson AL, Steinberg BM, Bonagura VR. 2020. Altered monocyte and langerhans cell innate immunity in patients with recurrent respiratory papillomatosis (RRP). Front Immunol 11:336. https://doi.org/10.3389/fimmu.2020.00336
5. Sin W-X, Li P, Yeong JP-S, Chin K-C. 2012. Activation and regulation of interferon-β in immune responses. Immunol Res 53:25–40. https://doi.org/10.1007/s12026-012-8293-7
6. Lau L, Gray EE, Brunette RL, Stetson DB. 2015. DNA tumor virus oncogenes antagonize the cGAS-STING DNA-sensing pathway. Science 350:568–571. https://doi.org/10.1126/science.aab3291
7. Samuel CE. 2001. Antiviral actions of interferons. Clin Microbiol Rev 14:778–809, https://doi.org/10.1128/CMR.14.4.778-809.2001
8. Parker BS, Rautela J, Hertzog PJ. 2016. Antitumour actions of interferons: implications for cancer therapy. Nat Rev Cancer 16:131–144. https://doi.org/10.1038/nrc.2016.14

9. Hoang TN, Viox EG, Upadhyay AA, Strongin Z, Tharp GK, Pino M, Nchioua R, Hirschenberger M, Gagne M, Nguyen K, et al. 2022. Modulation of type I interferon responses potently inhibits SARS-CoV-2 replication and inflammation in rhesus macaques. bioRxiv. https://doi.org/10.1101/2022.10.21.512606
10. Vozenin MC, Lord HK, Hartl D, Deutsch E. 2010. Unravelling the biology of human papillomavirus (HPV) related tumours to enhance their radiosensitivity. Cancer Treat Rev 36:629–636. https://doi.org/10.1016/j.ctrv.2010.03.010
11. Hoppe-Seyler K, Bossler F, Braun JA, Herrmann AL, Hoppe-Seyler F. 2018. The HPV E6/E7 oncogenes: key factors for viral carcinogenesis and therapeutic targets. Trends Microbiol 26:158–168. https://doi.org/10.1016/j.tim.2017.07.007
12. Stanley MA. 2012. Epithelial cell responses to infection with human papillomavirus. Clin Microbiol Rev 25:215–222. https://doi.org/10.1128/CMR.05028-11
13. Chen C, Xu P. 2023. Cellular functions of cGAS-STING signaling. Trends Cell Biol 33:630–648. https://doi.org/10.1016/j.tcb.2022.11.001
14. Poirson J, Suarez IP, Straub ML, Cousido-Siah A, Peixoto P, Hervouet E, Foster A, Mitschler A, Mukobo N, Chebaro Y, Garcin D, Recberlik S, Gaiddon C, Altschuh D, Nominé Y, Podjarny A, Trave G, Masson M. 2022. High-risk mucosal human papillomavirus 16 (HPV16) E6 protein and cutaneous HPV5 and HPV8 E6 proteins employ distinct strategies to interfere with interferon regulatory factor 3-mediated beta interferon expression. J Virol 96:e0187521. https://doi.org/10.1128/jvi.01875-21
15. Lou M, Huang D, Zhou Z, Shi X, Wu M, Rui Y, Su J, Zheng W, Yu XF. 2023. DNA virus oncoprotein HPV18 E7 selectively antagonizes cGAS-STING-triggered innate immune activation. J Med Virol 95:e28310. https://doi.org/10.1002/jmv.28310
16. Boulter N, Suarez FG, Schibeci S, Sunderland T, Tolhurst O, Hunter T, Hodge G, Handelsman D, Simanainen U, Hendriks E, Duggan K. 2016. A simple, accurate and universal method for quantification of PCR. BMC Biotechnol 16:27. https://doi.org/10.1186/s12896-016-0256-y
17. Dhanasekaran S, Doherty TM, Kenneth J, TB Trials Study Group. 2010. Comparison of different standards for real-time PCR-based absolute quantification. J Immunol Methods 354:34–39. https://doi.org/10.1016/j.jim.2010.01.004
18. Vu HL, Troubetzkoy S, Nguyen HH, Russell MW, Mestecky J. 2000. A method for quantification of absolute amounts of nucleic acids by (RT)-PCR and a new mathematical model for data analysis. Nucleic Acids Res 28:E18. https://doi.org/10.1093/nar/28.7.e18
19. Wu X, Xiao Y, Zhou S, Wang Y, Wang J. 2022. Transcriptomic landscape of gene expression profiles and pathways in juvenile-onset recurrent respiratory papillomatosis tumor tissues and human papillomavirus 6 and 11 E6- and E7-overexpressing head and neck squamous cell carcinoma cell lines. J Virol 96:e0134221. https://doi.org/10.1128/JVI.01342-21
20. Zhao C, Austin RM. 2007. Human papillomavirus DNA detection in ThinPrep PAP test vials is independent of cytologic sampling of the transformation zone. Gynecol Oncol 107:231–235. https://doi.org/10.1016/j.ygyno.2007.06.025
21. Fortes HR, von Ranke FM, Escuissato DL, Araujo Neto CA, Zanetti G, Hochhegger B, Souza CA, Marchiori E. 2017. Recurrent respiratory papillomatosis: a state-of-the-art review. Respir Med 126:116–121. https://doi.org/10.1016/j.rmed.2017.03.030
22. Schneider WM, Chevillotte MD, Rice CM. 2014. Interferon-stimulated genes: a complex web of host defenses. Annu Rev Immunol 32:513–545. https://doi.org/10.1146/annurev-immunol-032713-120231
23. Suttles J, Stout RD. 2009. Macrophage CD40 signaling: a pivotal regulator of disease protection and pathogenesis. Semin Immunol 21:257–264. https://doi.org/10.1016/j.smim.2009.05.011
24. Kletting S, Barthold S, Repnik U, Griffiths G, Loretz B, Schneider-Daum N, de Souza Carvalho-Wodarz C, Lehr C-M. 2018. Co-culture of human alveolar epithelial (hAELVi) and macrophage (THP-1) cell lines. Altex 35:211–222. https://doi.org/10.14573/altex.1607191
25. Donne AJ, Kinshuck A. 2021. Pharmacotherapy for recurrent respiratory papillomatosis (RRP): a treatment update. Expert Opin Pharmacother 22:1901–1908. https://doi.org/10.1080/14656566.2021.1935870
26. Goon P, Sauzet O, Schuermann M, Oppel F, Shao S, Scholtz LU, Sudhoff H, Goerner M. 2023. Recurrent respiratory papillomatosis (RRP)-meta-analyses on the use of the HPV vaccine as adjuvant therapy. NPJ Vaccines 8:49. https://doi.org/10.1038/s41541-023-00644-8
27. Bai K, Allen C. 2021. How enhancing immunity to low-risk HPV could cure recurrent respiratory papillomatosis. Laryngoscope 131:2041–2047. https://doi.org/10.1002/lary.29153
28. Wu X, Xiao Y, Guo D, Zhang Z, Liu M. 2022. Reduced NK cell cytotoxicity by papillomatosis-derived TGF-β contributing to low-risk HPV persistence in JORRP patients. Front Immunol 13:849493. https://doi.org/10.3389/fimmu.2022.849493
29. Luo X, Donnelly CR, Gong W, Heath BR, Hao Y, Donnelly LA, Moghbeli T, Tan YS, Lin X, Bellile E, Kansy BA, Carey TE, Brenner JC, Cheng L, Polverini PJ, Morgan MA, Wen H, Prince ME, Ferris RL, Xie Y, Young S, Wolf GT, Chen Q, Lei YL. 2020. HPV16 drives cancer immune escape via NLRX1-mediated degradation of STING. J Clin Invest 130:1635–1652. https://doi.org/10.1172/JCI129497
30. Yum S, Li M, Fang Y, Chen ZJ. 2021. TBK1 recruitment to STING activates both IRF3 and NF-κB that mediate immune defense against tumors and viral infections. Proc Natl Acad Sci U S A 118:e2100225118. https://doi.org/10.1073/pnas.2100225118
31. Hopfner KP, Hornung V. 2020. Molecular mechanisms and cellular functions of cGAS-STING signalling. Nat Rev Mol Cell Biol 21:501–521. https://doi.org/10.1038/s41580-020-0244-x
32. Uhlorn BL, Jackson R, Li S, Bratton SM, Van Doorslaer K, Campos SK. 2020. Vesicular trafficking permits evasion of cGAS/STING surveillance during initial human papillomavirus infection. PLoS Pathog 16:e1009028. https://doi.org/10.1371/journal.ppat.1009028
33. Gusho E, Laimins LA. 2022. Human papillomaviruses sensitize cells to DNA damage induced apoptosis by targeting the innate immune sensor cGAS. PLoS Pathog 18:e1010725. https://doi.org/10.1371/journal.ppat.1010725
34. Bortnik V, Wu M, Julcher B, Salinas A, Nikolic I, Simpson KJ, McMillan NA, Idris A. 2021. Loss of HPV type 16 E7 restores cGAS-STING responses in human papilloma virus-positive oropharyngeal squamous cell carcinomas cells. J Microbiol Immunol Infect 54:733–739. https://doi.org/10.1016/j.jmii.2020.07.010
35. Rodier C, Lapointe A, Coutlée F, Mayrand MH, Dal Soglio D, Roger M, Trottier H. 2013. Juvenile respiratory papillomatosis: risk factors for severity. J Med Virol 85:1447–1458. https://doi.org/10.1002/jmv.23615
36. Mounts P, Kashima H. 1984. Association of human papillomavirus subtype and clinical course in respiratory papillomatosis. Laryngoscope 94:28–33. https://doi.org/10.1002/lary.5540940106
37. Godínez JM, Nicolás-Párraga S, Pimenoff VN, Mengual-Chuliá B, Muñoz N, Bosch FX, Sánchez GI, McCloskey J, Bravo IG. 2014. Phylogenetically related, clinically different: human papillomaviruses 6 and 11 variants distribution in genital warts and in laryngeal papillomatosis. Clin Microbiol Infect 20O406–413. https://doi.org/10.1111/1469-0691.12420
38. Stanley M. 2006. Immune responses to human papillomavirus. Vaccine 24 Suppl 1:S16–S22. https://doi.org/10.1016/j.vaccine.2005.09.002
39. Santos LD, Antunes KH, Muraro SP, de Souza GF, da Silva AG, Felipe J de S, Zanetti LC, Czepielewski RS, Magnus K, Scotta M, Mattiello R, Maito F, de Souza APD, Weinlich R, Vinolo MAR, Porto BN. 2021. TNF-mediated alveolar macrophage necroptosis drives disease pathogenesis during respiratory syncytial virus infection. Eur Respir J 57:2003764. https://doi.org/10.1183/13993003.03764-2020
40. Ji JJ, Sun QM, Nie DY, Wang Q, Zhang H, Qin FF, Wang QS, Lu SF, Pang GM, Lu ZG. 2021. Probiotics protect against RSV infection by modulating the microbiota-alveolar-macrophage axis. Acta Pharmacol Sin 42:1630–1641. https://doi.org/10.1038/s41401-020-00573-5
41. Jablonska J, Leschner S, Westphal K, Lienenklaus S, Weiss S. 2010. Neutrophils responsive to endogenous IFN-beta regulate tumor angiogenesis and growth in a mouse tumor model. J Clin Invest 120:1151–1164. https://doi.org/10.1172/JCI37223
42. Zhou J, Huang J-D, Poon VKM, Chen D-Q, Chan CCS, Ng F, Guan X-Y, Watt RM, Lu L, Yuen K-Y, Zheng B-J. 2009. Functional dissection of an IFN-alpha/beta receptor 1 promoter variant that confers higher risk to chronic hepatitis B virus infection. J Hepatol 51:322–332. https://doi.org/10.1016/j.jhep.2009.03.020